Available online at www.sciencedirect.com
SCIENCE DIRECT®
International Journal of Heat and Fluid Flow 25 (2004) 223–242
International Journal of HEAT AND FLUID FLOW
www.elsevier.com/locate/ijhff

Heat transfer characteristics and mechanisms along entire boiling curves under steady-state and transient conditions

H. Auracher [a,*], W. Marquardt [b]

[a] Institut für Energietechnik, Technische Universität Berlin, Marchstr. 18, D-10587 Berlin, Germany
[b] Lehrstuhl für Prozesstechnik, RWTH Aachen, Turmstr. 43, D-52064 Aachen, Germany

Abstract

The paper presents a survey of results found by the authors and their groups during recent years. An experimental technique for precise and systematic measurements of entire boiling curves under steady-state and transient conditions has been developed. Pool boiling experiments for well wetting fluids and fluids with a larger contact angle (FC-72, isopropanol, water) yield single and reproducible boiling curves if the system is clean. However, even minimal deposits on the surface change the heat transfer characteristic and shift the boiling curve with each test run. The situation is different under transient conditions: heating and cooling transients yield different curves even on clean surfaces. Measurements with micro-optical probes give an insight in the two-phase dynamics above the heating surface in the different boiling regimes. Temperature signals from microthermocouples at the surface and the optical probe data lead to some conclusions on the physics of boiling in different regimes such as the macrolayer configuration, the dry-spot size and dynamics, the nucleation site density etc. The high density of active nucleation sites in the region between fully developed nucleate boiling and critical heat flux (CHF) and the resulting highly turbulent two-phase boundary layer let us conclude that the strong increase of heat flux in heating transients and vice versa in a cooling process is mainly due to the intensive two-phase convection heat transfer from the wall to the bulk and not due to inertia effects in the two-phase structure dynamics. The latter is not significantly affected by temperature transients. An interfacial-area-density model is proposed. It needs data from the optical probes and enables the prediction of entire boiling curves by employing only one fitting parameter. Furthermore the concept of a reaction–diffusion model is presented to predict CHF. Here the triggering of CHF is due to an instability of dry spots on the heating surface. Data from microthermocouples and optical probes are needed to evaluate this model. Many aspects of the extremely complex mechanisms of boiling are still not sufficiently understood. The problems should be tackled from both the experimental and the theoretical end and both approaches should be closely linked.

Keywords: Microthermocouple; Optical probe; Pool boiling; Transition boiling; Surface wetting; Dry patch; CHF; Surface temperature; Boiling mechanism; Interfacial velocity

1. Introduction

Empirical correlations to predict heat transfer in boiling still govern the field. Their disadvantage is well known: the limited range of validity. They are only reliable for system conditions very close to the experiments from where they originate. Taking into account the huge number of parameters and properties affecting heat transfer in boiling, the number of necessary experiments to provide a complete set of empirical correlations would approach infinity.

A significant reduction of the number of experiments—which are unavoidable in boiling research—can be expected if we focus our studies to the governing mechanisms of this very complex process. Basic mechanisms such as bubble dynamics are rather well understood and in recent years the microlayer theory was an important step forward to predict boiling heat transfer at lower heat fluxes where no significant interaction between the bubbles occur. But at higher heat fluxes up to the critical one and beyond it our understanding of the mechanisms is not advanced. Models as the macrolayer theory, Zuber's hydrodynamic theory or

* Corresponding author. Tel.: +49-30-314-25710; fax: +49-30-314-21779.
E-mail address: auracher@iet.tu-berlin.de (H. Auracher).

0142-727X/$ - see front matter © 2003 Elsevier Inc. All rights reserved.
doi:10.1016/j.ijheatfluidflow.2003.11.011

Nomenclature

A_i	interfacial area density
C_{CHF}, C_1	constants
c	specific heat capacity
CHF	critical heat flux
f	contact frequency
Δh_v	latent heat of evaporation
Ja	Jacob number
L_i	interfacial contact line density
q	heat flux
ΔT	wall superheat, $T_w - T_{sat}$
α_v	void fraction, vapor fraction
β	distance between dry spots
2δ	dry spot size
$\bar{v}_C$	average interfacial velocity
Φ	contact angle
ρ	density
ϑ	temperature

Subscripts

L	liquid
v	vapor

Berenson's proposal to correlate transition boiling are first approaches or interesting ideas but they are not well supported by experiments and/or do not take into account important parameters.

One of the reasons for this unsatisfactory situation is that sophisticated experimental techniques are required to study the mechanisms of boiling in the higher wall superheat regions. Non-intrusive techniques are not applicable. We therefore need miniaturized sensors which do not significantly disturb the processes taking place inside and above the heater. Furthermore highly powerful data acquisition systems are required with high resolution to accurately analyze fast transients such as temperature drops in the heater near the surface if a liquid contact or interface movements occur in the two-phase layer above the heater.

Moreover, the application of sophisticated experimental techniques is only one requirement towards more generally valid, mechanistically based prediction methods. We also need the cooperation with experts in modeling and numerical solution of complex processes. The cooperation of experimentalists and theorists should be closely linked and start already during the creation of experiments in terms of model-based experimental design. Since the high complexity of the boiling process can neither be modeled nor experimentally be verified in all details, the objective should be to create models in not much more detail than experimentally accessible. Both authors try to follow the lines mentioned above. The group in Berlin is focused on experimental work and the one in Aachen on theoretical problems. The objective of the present report is to present a summary of results found by our groups in very close cooperation during the past years.

First an experimental technique is presented which enables a precise and systematic measurement of entire boiling curves under steady-state and transient conditions. This technique has been applied, in the first step, to find out whether boiling curves exhibit a hysteresis in the transition region under steady-state conditions. To find an answer, steady-state experiments were carried out with well wetting fluids and fluids with a larger contact angle (FC-72, isopropanol, water). Moreover, boiling curves under transient heating and cooling conditions have been determined with FC-72. Here, the heating and cooling rate was varied systematically. A precise technique to determine entire boiling curves is a necessary prerequisite to study the boiling mechanisms in the different boiling regimes. Results of this kind are presented in a second part of the present report. Micro-optical probes were applied to study the two-phase behavior above the heating surface in the different boiling regions. Microthermocouples beneath the surface were used to measure temperature fluctuations caused by the two-phase dynamics above the surface.

All the obtained results lead to some conclusions on the mechanisms of boiling such as the macrolayer configuration, the dry spot size and dynamics, the nucleation site density etc. These findings and others from the literature are used as input to physically based boiling heat transfer models which are proposed in the last part. Firstly an interfacial-area-density model is proposed to determine entire boiling curves based on data from the optical probes. Secondly a reaction–diffusion model is presented to predict critical heat flux (CHF). It needs information about the dry spot behavior on the heating surface.

2. Experimental facilities

Details of the main experimental facilities are already described by Auracher and Marquardt (2002). However, it seems necessary to present at least a summary and to add information about new devices in more detail.

2.1. Test loop

Fig. 1 shows the test loop used for pool boiling experiments. It consists of a boiling vessel (diameter 209

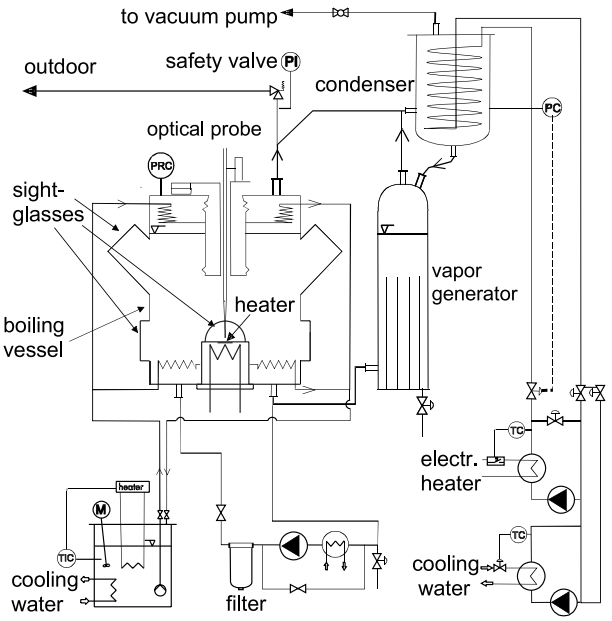

Fig. 1. Test loop.

mm, height 332 mm), a vapor generator, a condenser and a filter loop. Maximum possible operating pressure is 1.0 MPa. In water and isopropanol tests, the generator provides a basic load for the condenser and reheats subcooled liquid from the condenser to insure constant saturation state at the vessel inlet. A recirculated temperature controlled bath is used to keep constant saturation conditions in the vessel via two tube coils. In FC-72 experiments the vapor generator is not needed. Four sightglasses at heater level and two at an angle of 45° enable observation of the boiling process. Optical probes are installed on the top of the vessel. They are 3D-moveable by a micrometer and a piezo-electric adjusting device. The complete test loop is made from stainless steel, pickled, electropolished and passivated.

2.2. Test heaters

2.2.1. Model-based heater design

For the design of the test heaters, several competing and contradicting design criteria have to be considered to allow for a save operation of the apparatus and to conduct meaningful boiling experiments. To meet these design objectives optimally a model-based design approach has been applied which includes 2- and 3D FEM simulations of the temperature field and stability analyses of the controlled apparatus (more details in Blum et al., 1996; Buchholz et al., 2000; Hohl et al., 2001).

2.2.2. Pool boiling experiments with water and isopropanol

An outline of the heater section shows Fig. 2. The copper heater with surface diameter of 35 and 8 mm

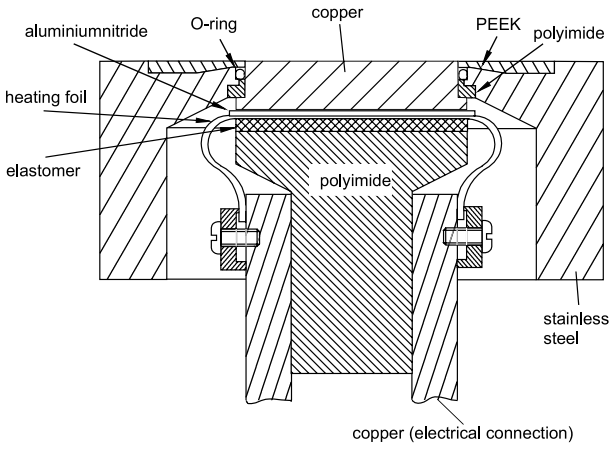

Fig. 2. Heater for experiments with water and isopropanol.

thickness is fixed in a stainless steel housing. The copper block is cylindrical in the top part and quadratic in the bottom part with the edges cut off (more details in Buchholz et al., 2000). The quadratic shape is needed to enable heating by a 25 μm thick heating foil pressed onto the bottom. An aluminium nitride plate between foil and heater serves as electrical insulator. The maximum possible heat flux at the heater surface is 5.5 MW/m^2 with a maximum heating current of 350 A. 12 K-type thermocouples (∅ 0.25 mm) with the tips 1.3 mm below the surface were implanted in the heater by electroplating. They are used for temperature control, over temperature protection and the determination of the average surface temperature.

The surface temperature fluctuations are measured by several microthermocouples with the tips (copper/constantan) at a distance of 13 μm to the surface, Fig. 3. In

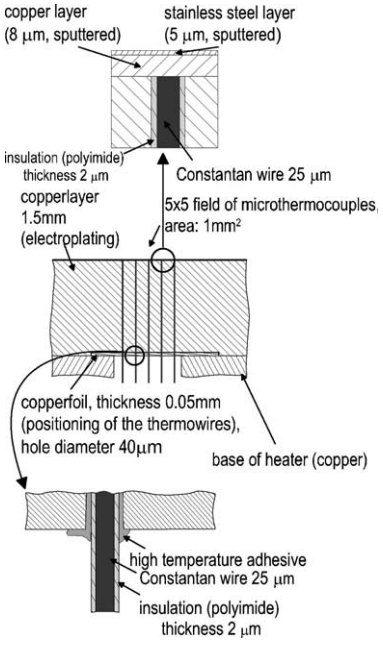

Fig. 3. Installation of microthermocouples.

the center of the heater surface a grid of 5×5 sensors (∅ 25 μm) is installed within an area of 1 mm^2, Fig. 4. This grid is surrounded by three quadratic arrays of eight microthermocouples (∅ 50 μm) each, more details in Buchholz et al. (2001). The heater surface was fine-sandblasted. A topographic view of the region above the 5×5 grid (Fig. 4), measured by 3D topography, shows that the microthermocouples do not affect the surface structure (more details in Luke and Gorenflo, 2001).

2.2.3. Pool boiling experiments with FC-72

Two heaters are used for the experiments with FC-72 (C_6F_{14}, 3-M company), one for steady-state and the other for transient experiments. They are similar except for the size and the heating mode. For steady-state experiments a copper heater (no. 1) with 34 mm diameter and 10 mm thickness, DC-heated indirectly from the bottom by a sheathed resistance wire, was applied (more details in Hohl et al., 1998). For the transient experiments a heater (no. 2) with lower thermal inertia and higher maximum heat input was used (Fig. 5). The design of this heater is similar to the one used for the water and isopropanol experiments (Fig. 2). It consists of a 5 mm thick copper block, 20×20 mm squared in the bottom part and cylindrical with 18.2 mm diameter in the top part. It is insulated ($\lambda = 0.22$ W/m/K) and sealed by polyimide. Heat losses through the polyimide block are small, hence one-dimensional heat conduction can be assumed. Three thermocouples of 0.25 mm outer diameter and a number of microthermocouples are also installed in heater no. 2 (more details in Hohl and Auracher, 2000).

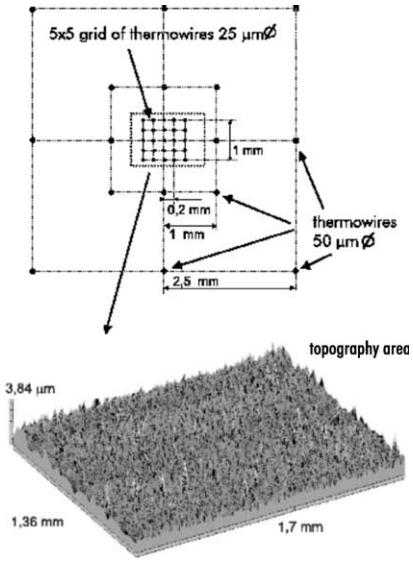

Fig. 4. Distribution of thermocouples and surface topography.

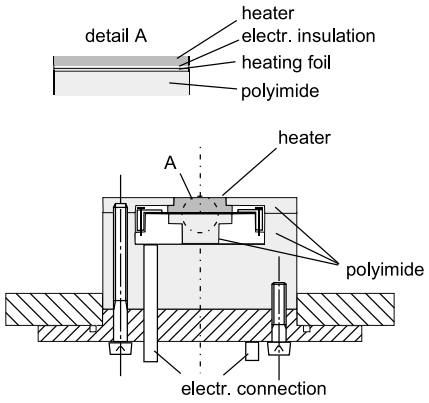

Fig. 5. Heater (no. 2) for experiments with FC-72.

2.3. Control concept and stability analysis

The wall temperature is controlled by measuring the temperature close to the boiling surface, comparing it to a setpoint value which is either constant in steady-state experiments or time-varying in transient experiments, feeding the difference signal into the controller and adjusting the power of the electric heating according to the controller output. The setpoint signal as well as the control law are implemented on a computer. More details for the steady-state and the transient experiments with FC-72 are presented by Hohl et al. (2001).

The access to the transition region in the case of water experiments and to a certain extent also in the isopropanol tests is more difficult than with FC-72 because of the high heat fluxes and the steep negative slope of the boiling curves. A stability analysis has been performed based on the Laplace domain transfer function model of the test heaters, i.e., the one-dimensional heat conduction equation and all control loop elements. Solving for the poles of the closed-loop system numerically, the stability limits of the controlled system can be found (more details in Blum et al., 1996).

2.4. Data acquisition and measurement evaluation

2.4.1. Water and isopropanol pool boiling experiments

Heating voltage, heating current and amplified temperature signals of the K-type thermocouples are sampled with the data acquisition board PC30 (Meilhaus Electronic). For the isopropanol experiments, this card has been replaced by two DaqBoard2000 cards (IO-Tech). The sampling frequency for each channel is 100 Hz. The amplified voltages of the microthermocouples are sampled at a rate of 12.5 kHz for each channel by the DSP-controlled data acquisition board ADC-64 for PC (32 channels, 16 Bit, Innovative Integration). Groups of eight channels are acquired simultaneously and a special software enables to sample all channels in burst mode to achieve almost simultaneous sampling of

all channels. The maximum time difference between the first and last sampled group is less than 20 μs.

Heater temperature control is realized by the digital signal processing board AT-DSP 2200 (National Instruments). The discrete PI-controller runs on the onboard DSP-processor. The total time between stimulus and response at the output of the card is 1.5 ms. The input heater temperature used for the temperature controller is the instantaneous average of 12 sheathed thermocouples in the test heater. The output voltage of the card is amplified and supplied to the heating foil. The surface superheat is calculated by correcting the time average of the temperature measured by thermocouples by the temperature difference between sensor location and heating surface, assuming a one-dimensional temperature field in the test heater. The same holds for the steady-state experiments with FC-72.

2.4.2. FC-72 experiments

In the steady-state case data are sampled for 2 s for each point of the boiling curve. The entire boiling curve is recorded by successively raising or lowering the set-point value. In transient experiments, the controller must additionally track a prescribed temperature trajectory. Here, a ramp with the temporal gradient as the varied parameter and as a measure for transient dynamics is chosen. The sampling frequency for each channel is chosen to be 200 Hz during steady-state experiments, 500 Hz during slow transients up to 15 K/s and 5000 Hz during fast transient runs. In transient experiments, both heat flux and temperature at the heater surface are calculated by means of an inverse heat conduction algorithm presented by Hohl et al. (2001).

2.5. Optical probes

2.5.1. FC-72

To investigate the liquid–vapor fluctuations above the heater, fiber-optic probes have been developed. In the FC-72 experiments one single probe was used. It consists of a gradient index glass fiber with the end of the fiber formed into a conical shape. This was done by melting the tip under a microscope with a small burner. The fiber was then glued into small stainless steel tubes with increasing diameter to make it sufficiently stiff. The probe tip diameter is only 10 μm. The probe can be moved at different heights and different locations above the heater by means of a 3D-micrometer adjusting device (see Fig. 1). More details of this technique are presented by Hohl (1999).

2.5.2. Isopropanol

Recently Buchholz et al. (2004) developed improved optical probes which were used in experiments with isopropanol. The probes are made from single mode quartz glass fiber with a cladding diameter of 125 μm and a core diameter of 8 μm. The tip of the probe is formed by etching in hydrofluoric acid. This method enables the preparation of very small probe tips. Measurements with a scanning electron microscope shows a tip diameter of less than 1.5 μm (Fig. 6).

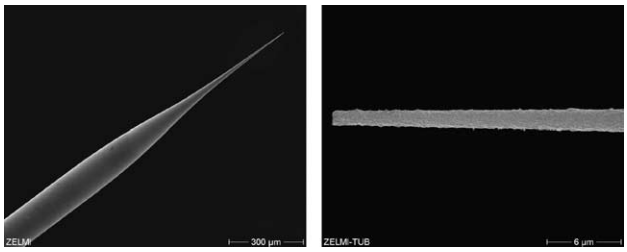

Fig. 6. Scanning electron microscope photograph of the optical probe.

The probe is 3D-moveable by means of micrometer stages. The position perpendicular to the test heater is measured both with the precision stage and a precision linear variable displacement transformer with an accuracy of ±1.1 μm.

Four of these optical probes have been combined to form a 4-tip multiple probe. The optical fibers are placed next to each other (125 μm between each in radial direction) with different axial distances. The distances to the lower probe are 160, 420 and 750 μm. Additionally a stainless steel wire with 50 μm diameter is fixed to the probe ensemble with a radial distance of approximately 800 μm and a given distance to the lower probe tip. If an electrical contact occurs between the wire and the heater surface the desired optical probe distance to the surface is reached.

One of the ADC-64 cards (see Section 2.4) was used for data acquisition with a sampling rate of 200 kHz per channel. A 1-min run at full 200 kHz generates about 800 MB ASCII-data. More information about the optical probe technology is presented by Buchholz et al. (2004).

3. Results

3.1. Steady-state pool boiling experiments with FC-72, water and isopropanol

3.1.1. FC-72

Fig. 7 shows a boiling curve of FC-72 measured with heater no. 1 under steady-state conditions. The test fluid was saturated at 333 K corresponding to a pressure ratio of $p/p_{cr} = 0.071$ (critical pressure $p_{cr} = 1.83$ MPa).

The experiments were carried out with stepwise increasing and decreasing heater temperature. In contrast to Witte and Lienhard's (1982), postulation, no hysteresis was observed in the transition region. However, it should be mentioned, that in agreement with Ungar and Eichhorn's (1996), observation,

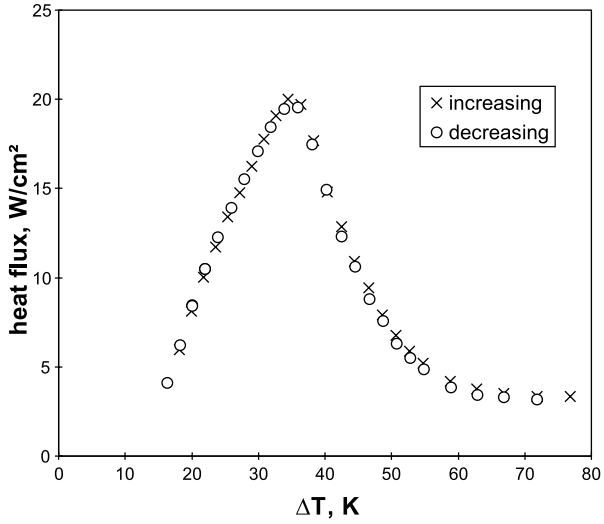

Fig. 7. Steady-state boiling curve of FC-72 ($p = 0.13$ MPa; $p/p_{cr} = 0.071$; more details in Hohl, 1999).

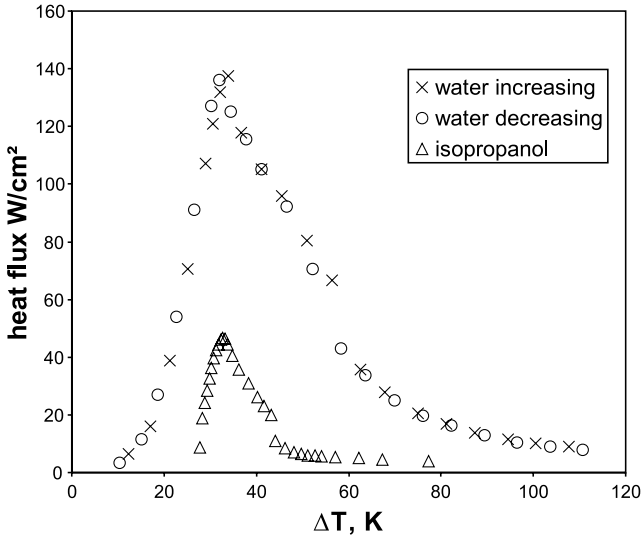

Fig. 8. Steady-state boiling curves of distilled water (0.1 MPa, $p/p_{cr} = 0.0045$) and isopropanol (0.12 MPa, $p/p_{cr} = 0.025$).

contamination during the steady-state experiments can shift the boiling curve. This was the case in preliminary experiments prior to the final cleaning of our test apparatus.

Some authors assumed that the results from our small heater are not representative because of the similarity of the heater diameter and the most dangerous Taylor wavelength. This is, however, not likely since the diameter of heater no. 1 is 4.3 times larger than this wavelength (7.9 mm for FC-72 at 60 °C). It was furthermore mentioned that a hysteresis is not observed because of the small contact angle between FC-72 and nickel. For clarification we carried out experiments with water, where the contact angle is significantly larger than with FC-72.

3.1.2. Water

The experiments were performed at atmospheric pressure ($p/p_{cr} = 0.0045$) with distilled water. It was carefully cleaned and degassed and several preliminary runs to clean the inner surfaces of the test loop have been carried out prior to the final experiments. A typical result is shown in Fig. 8. This boiling curve was measured with stepwise decreasing temperature from a starting point in the film boiling regime to low heat flux nucleate boiling. Afterwards, the heater temperature was increased stepwise starting in nucleate boiling until film boiling was reached again. The heater temperature control was able to stabilize the boiling process in all boiling regimes. All points of the boiling curve were measured under steady-state conditions.

No distinct hysteresis in the transition boiling regime can be identified. However, a small disturbance in the shape of the otherwise smooth curve is recognizable at a ΔT of about 55 K in Fig. 8. A similar but even smaller effect can be observed in the transition boiling region of isopropanol at $\Delta T \approx 43$ K (plotted also in Fig. 8). Our microthermocouples indicate that non-uniform boiling effects may cause these slight alterations of the boiling curve shape. Via the temperature distribution we indirectly observed larger clusters of dry patches on the surface which change their configuration with the wall superheat leading to the above mentioned disturbance. The size of the clusters is still smaller than the heater surface area but they are large enough to disturb the ergodic behavior of the boiling mode across the surface. In the measurements with FC-72 we did not observe this kind of disturbance. The effect is obviously the more pronounced the higher the heat flux is. Maybe also the contact angle, which increases from FC-72 via isopropanol to water, has an effect. We are not yet able to give a physical/mathematical explanation of this clustering effect in the transition region during steady-state experiments.

Fig. 9 shows boiling curves for power station feedwater on a surface with deposits. After approximately 30 s boiling at CHF to activate the nucleation sites on the heater and a subsequent decrease of the wall temperature, the heater temperature was increased stepwise from nucleate to film boiling and back vice versa. The shape of the boiling curve changed significantly during the experiment. Mostly, the boiling curve shifts to higher heat fluxes and the superheat at CHF decreases. The effect is similar to that one observed by Ungar and Eichhorn (1996). During the measurement the boiling surface changed remarkably. An opaque layer of a white, hard substance built up on the heater. The disturbance of the boiling curve shown in Fig. 9 is not a result of insufficient reproducibility caused by the

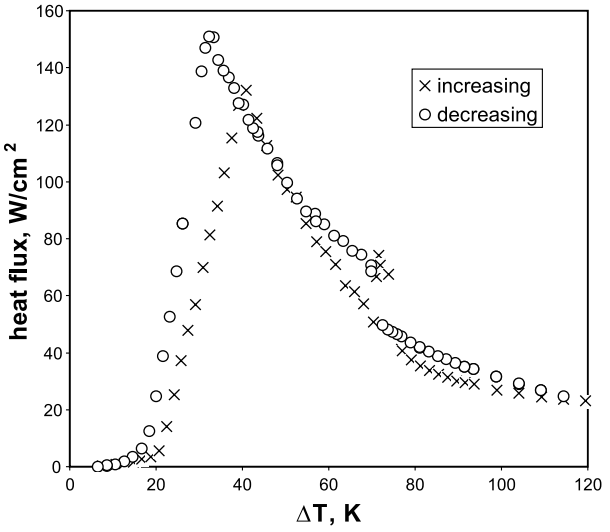

Fig. 9. Boiling curves of power station feedwater on a surface with deposits at 0.1 MPa ($p/p_{cr} = 0.0045$). More details in Buchholz et al. (2000).

experimental facility itself, it is obviously a result of the continuously growing deposit on the surface. Reducing all possibilities which may lead to deposits to a minimum, e.g. insufficient purity of the test liquid, long measurement duration, insufficient cleaning of the boiling vessel and other parts of the loop in contact with the test fluid etc., leads to reproducible boiling curves as plotted in Fig. 8. On the other hand our experience is, especially with water, that boiling curves are very sensitive to contamination of the boiling surface in terms of reproducibility.

Incidentally there is no indication that the above mentioned contamination effect is in any connection to the dry spot clustering effect in the transition region mentioned in the previous paragraph. It is also unlikely that this clustering effect is caused by insufficient controlling. In this case we would have either harmonic oscillations of the average surface temperature or a transition of this temperature to a stable operating point on the boiling curve (more details in Blum et al., 1996). Finally it should be mentioned that the most dangerous Taylor wavelength is 19 mm for boiling water at 0.1 MPa and hence, as in the FC-72 experiments, much smaller than the heater diameter.

3.1.3. Isopropanol

The tests with isopropanol were carried out in a pressure range between 0.033 MPa ($p/p_{cr} = 0.007$) and 0.332 MPa ($p/p_{cr} = 0.07$). Hence, the system was—in contrast to the water experiments—closed to the atmosphere. As with the other fluids reproducible boiling curves could only be obtained with a carefully purified liquid and a clean surface. In this case again no hysteresis was observed between curves measured with stepwise increasing and stepwise decreasing temperature, respectively. An example is plotted in Fig. 8.

3.2. Transient pool boiling experiments with FC-72

3.2.1. Boiling curves for transient heating

Boiling curves for transient heating with up to 50 K/s nominal temperature change per second of the heating surface measured with heater 2 (Fig. 5) are depicted in Fig. 10. These curves represent heat fluxes and temperatures at the heater surface determined by solving the inverse heat conduction problem. For comparison, the steady-state boiling curve is also measured with stepwise increasing and decreasing temperature and again no hysteresis was observed. This curve deviates a little from the one in Fig. 7. The main reason is that we did not take into account precisely the heat losses of the different heaters. Consequently, some small errors are also included in the determination of the surface temperature. Since these errors have no influence on the qualitative shape of the boiling curves, we made no further correction of the plotted data. All experiments were carried out in a way that nucleation sites were already active at the start of heating ($\Delta T \approx 15$ K) to avoid the disturbance effect of boiling incipience.

Details of the transient experiments are presented by Hohl et al. (2001). Summarizing, the following main results were obtained:

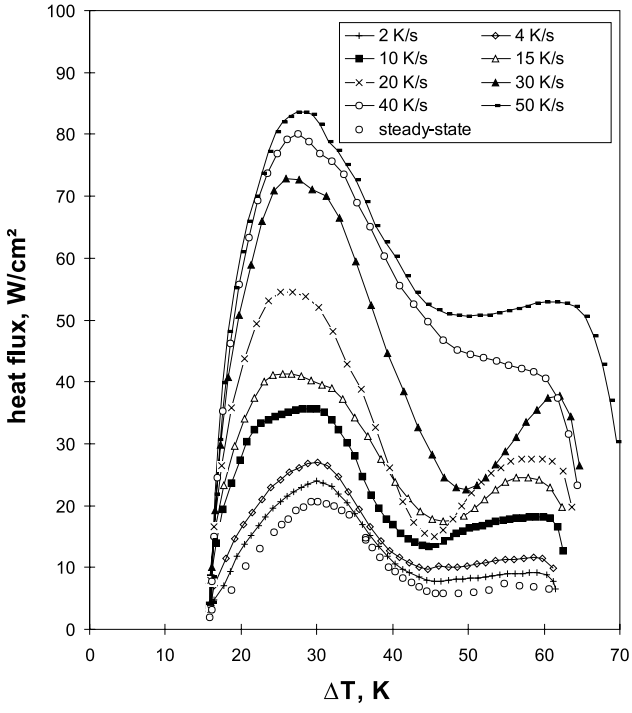

Fig. 10. Boiling curves of FC-72 for transient heating at 0.13 MPa ($p/p_{cr} = 0.071$). More details in Hohl et al. (2001).

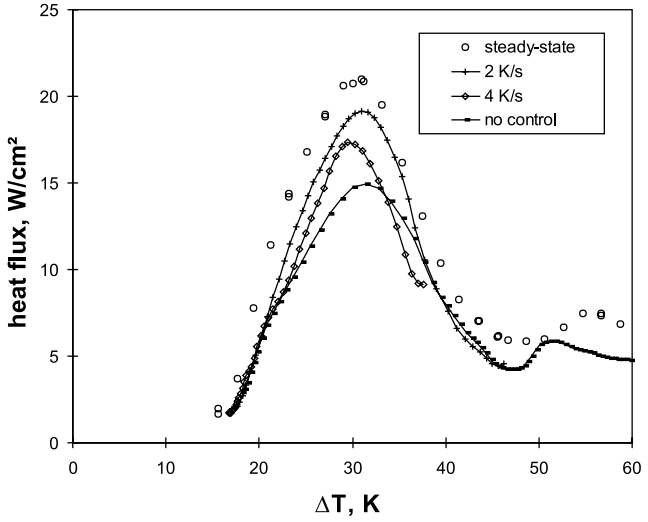

Fig. 11. Boiling curves of FC-72 for transient cooling at 0.13 MPa ($p/p_{cr} = 0.071$). More details in Hohl et al. (2001).

- The heat flux increases strongly with increasing heating rate. At 50 K/s, the critical heat flux (CHF) is by a factor 4 larger than the one in the steady-state case. The superheat at CHF does not change remarkably with the heating rate.
- The minimum heat flux of film boiling (MHF) does not exhibit a clear trend. The heat flux in film boiling during the heating mode is significantly higher than in steady-state heating. After switching off the heating power to start the cooling mode somewhere between a superheat of 60 and 70 K the heat flux drops down to at least the value of the steady-state case (see Fig. 11).
- The behavior shown in Fig. 10 (and Fig. 11 as well) is not due to an evaluation uncertainty or error. An energy balance reveals that the inverse heat conduction problem is solved properly. The boiling curve characteristic in transient heating shown in Fig. 10 is due to a physical effect of the boiling mechanism. This holds also for transient cooling (Fig. 11).

3.2.2. Boiling curves for transient cooling

Due to the thermal inertia of the heater the cooling rate is limited. Constant cooling rates were only possible for 2 K/s along the entire boiling curve and for 4 K/s between transition and nucleate boiling (see Fig. 11). With zero heat input, the cooling rate was about 2 K/s in film boiling and 6.8 K/s in the CHF region. Obviously, the transient cooling effect is contrary to the transient heating behavior (note that the steady-state curve in Fig. 11 is the same as the one in Fig. 10). The faster the cooling rate the smaller the heat flux. Keys to a physical explanation of the transient boiling mechanisms are data obtained from optical probes and microthermocouples discussed later in this report.

3.3. Experiments with microthermocouples

3.3.1. FC-72

The experiments with FC-72 were carried out with heater no. 2 (Fig. 5). It contains also a bunch of microthermocouples, however, with a somewhat different geometrical configuration than those in the heater for isopropanol and water experiments (Figs. 2–4). Details of these experiments are presented by Hohl and Auracher (2000).

Searching for an explanation of the strong difference between steady-state and transient heat transfer data (Section 3.2) we carried out standard statistical analyses of the temperature fluctuations measured with this type of microthermocouples along the entire boiling curve of FC-72 in steady-state and transient experiments. The analyses led us to the following conclusions.

Up to CHF no significant difference in signal characteristics occurring at a given wall superheat in steady-state or transient runs is observed. If the wall superheat increases further the temperature amplitudes also increase but now a delay in amplitude amplification can be observed in heating transient runs, i.e., in the transition region the instantaneous temperature amplitudes at a given wall superheat are smaller in transient runs than in a steady-state measurement. An analogous conclusion holds probably for the cooling mode, but the transients were not fast enough for a clear observation. Hence, it seems that no significant difference in the wetting mechanisms exists under steady-state and transient conditions at the same wall superheat up to about CHF. Beyond CHF, however, a delay effect in the liquid–vapor fluctuations seems to occur. In transient heating the two-phase structure formation above the heating surface may not be sufficiently fast to follow a fast transient.

The above conclusion for the nucleate boiling region is not surprising. At a bubble departure frequency of, say, 100 Hz, the temperature rise of the heater surface during the period between two bubbles is only 0.5 K at the fastest transient of 50 K/s (Fig. 10). Hence in a first approach we may argue that since vapor generation and wetting mechanism are much faster processes than the change of the average temperature with time during a transient, the vapor/liquid structure close to the heater surface region for a given ΔT is not strongly influenced by the transient. Consequently the strong influence of transients on the heat transfer is at least in the nucleate boiling region not primarily due to a change in the two-phase characteristics above the heater surface. A more reasonable explanation is given in Section 5.1.

3.3.2. Isopropanol

Temperature fluctuations detected by the microthermocouples are indicators for the wetting/dryout dynamics on the heater surface. Final objective of these

measurements is to obtain a good temporal and spacial resolution of temperatures and heat fluxes at the surface and hence information on bubble dynamics, dry spot behavior etc. Since the sensor tips are 13 μm beneath the surface a 3D inverse heat conduction problem (IHCP) has to be solved to estimate the surface data. This type of evaluation has been carried out by Buchholz et al. (2001), with isopropanol boiling on the heater shown in Fig. 2.

The microthermocouple arrangement is depicted in Figs. 3 and 4. Typical temperature signals, simultaneously measured by sensors 25 and 26, are plotted in Fig. 12. The sensor locations are indicated by bold numbers in Figs. 13 and 14, respectively. The mean heat flux during this measurement was 8.5 W/cm^2 in the transition region, not far from film boiling (see boiling curve in Fig. 8). Periods of high temperature are interrupted by extremely fast and short temperature drops with a more or less different characteristic at the two sensors. At the falling branch, temperature transients of more than 6000 K/s can be observed (an improved version of microthermocouple arrangement and data sampling, presented by Buchholz et al. (2004), shows that temperature drop rates of more than 10,000 K/s occur). A heat flux necessary to generate such rapid temperature changes is most likely caused by a local rewetting of the surface by cold bulk liquid. After the drastic drop of the temperature it only gradually reaches the initial level again.

The measured temperature field is plotted in Fig. 13 for two time instances with 0.16 ms between each. The temperatures between the measured ones have been interpolated by cubic functions. The dashed rectangular area in the upper plot of Fig. 13 depicts the area of the 3D-IHCP calculations presented in later paragraphs (see also Fig. 14). The two plots in Fig. 13 show on the right

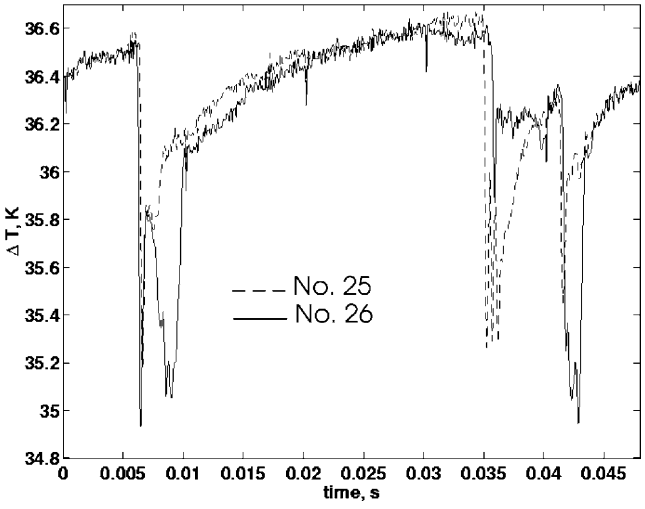

Fig. 12. Typical temperature signals from thermocouples 25 and 26 (see Figs. 13 and 14).

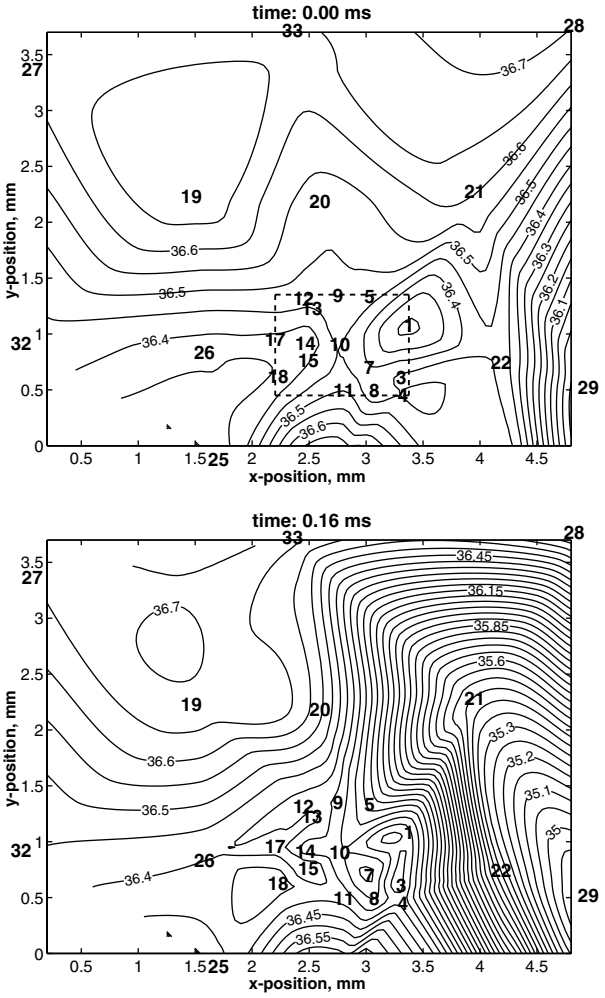

Fig. 13. Temperature field 13 μm beneath the heater surface (isopropanol; transition region).

hand side a moving surface wetting. Near to thermocouple 29 a temperature gradient can be seen most likely caused by a rewetting spot. The temperature decrease moves to the left and covers after only 0.16 ms about 1/3 of the area of consideration. A large number of plots as shown in Fig. 13 can be generated from the measured data. These plots give a good picture of the wetting/dryout dynamics in terms of size, distribution and frequency of dry spots in the different boiling regions (new results are presented by Buchholz et al., 2004).

Using the measured temperature data taken by the microthermocouples inside the heater, the spatially and temporal heat fluxes at the surface were estimated by solving an inverse heat conduction problem. Inverse problems are mathematically ill-posed in the sense of Hadamard: The solution is not unique, small perturbations in the data lead to large deviations in the estimated quantities and the solution does not depend continuously on the data. In order to get a useful approximate solution of noisy measurements, regularization of the ill-posed problem is necessary. In Buchholz et al. (2001), a

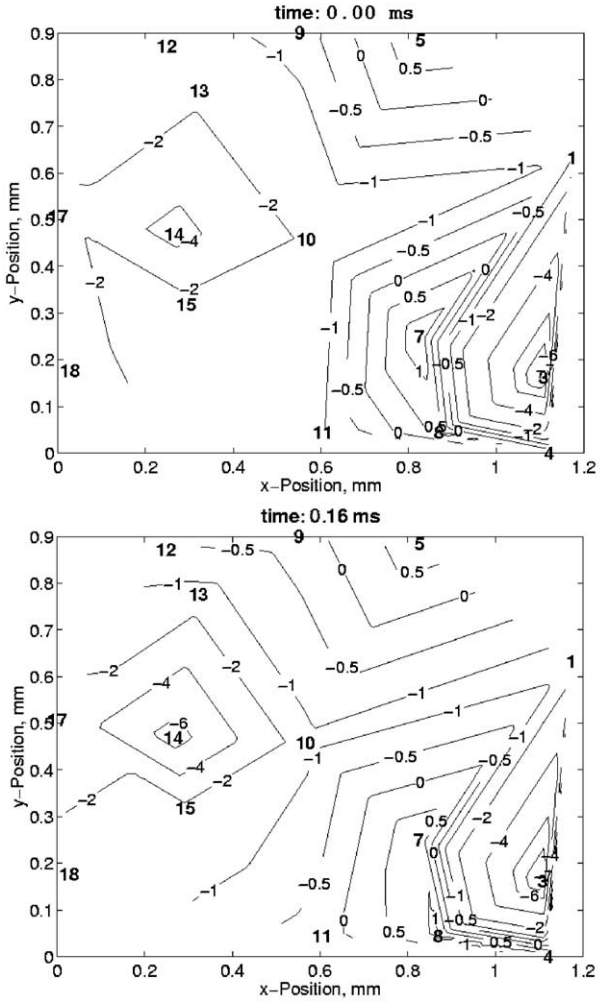

Fig. 14. Estimated heat flux field from the surface to isopropanol (negative numbers) in MW/m^2.

modification of the method developed by Blum and Marquardt (1997a,b) was used to extend the algorithm to problems with complex geometry and to address numerical efficiency. The basic idea is to use a transfer matrix model followed by low-pass filtering to generate a stable, approximate inverse. The lowpass-filtering has been performed using a Chebycheff Filter of order 15 with a cut-off frequency of 400 Hz. The order, cut-off frequency, and type of filtering was determined on the basis of signal noise, model approximation and stable approximation of the inverse. In order to obtain a transfer function matrix model of the heater, (1) a 3D-state space model of the heater was generated by the FE-method, (2) the unknown boundary heat fluxes were parameterized using linear functions, (3) the model was reduced using the numerical routines in SLICOT (Varga, 1999) and (4) the exact model inverse was calculated using a system theoretic approach by Silverman (1969). Then the IHCP was solved as proposed by Blum and Marquardt (1997a,b).

The estimated surface heat fluxes are shown exemplarily in Fig. 14. A different sequence of the signals as plotted in Fig. 13 is shown here. A local heat flux increase to approximately $|6\ \mathrm{MW/m^2}|$ can be exhibited around thermocouple 14 probably due to liquid contact with the surface and immense evaporation. Around thermocouple 3 one can observe a similar heat flux spot already residing for a little longer time. Buchholz et al. (2001) mention that their method to estimate the surface heat fluxes is not yet satisfactory. The fluctuations induced by boiling contain much higher frequency signal parts (up to ≈3000 Hz) than the cut-off frequency of the filter used in the estimation procedure. Thus high-frequent characteristics of the heat fluxes are not preserved in the estimates. Due to this, one can expect the real local heat fluxes to be of much higher amplitude than shown here. It is also not clear whether heat fluxes from the fluid to the heater can occur (see the few positive numbers in the plots of Fig. 14). In order to improve the procedure the spatial discretization of the FEM-model must be further increased which means that adaptive solution methods have to be developed as numerical restrictions prohibit simple reduction of grid size.

3.4. Experiments with optical probes

3.4.1. FC-72

Experiments with FC-72 have been carried out with heater no. 1 and the probe with 10 μm tip diameter under steady-state conditions. Details are presented by Hohl et al. (1998). Outcome of these measurements are e.g. void fractions and vapor contact frequencies as a function of the distance to the heater. A typical result for the void fraction distribution is plotted in Fig. 15.

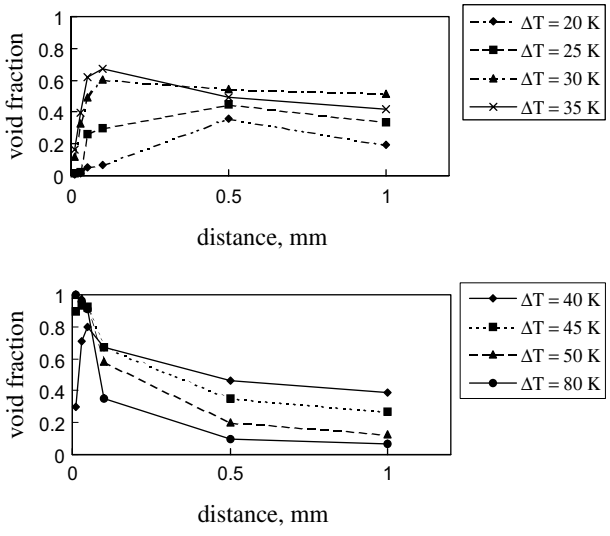

Fig. 15. Time averaged void fraction of FC-72 above heater in different boiling regimes.

Measurements were carried out at the center of the heater at distances of the probe tip from the heater surface between 0.01 and 1 mm. The distance was determined with an accuracy of ±0.01 mm by measuring the signal rise as a result of light reflection at the heater surface when the probe comes very close to it. In measurements at 0.01 mm nominal distance from the heater, it can be assured that the probe tip was fixed within a real distance between 0.005 and 0.02 mm from the heater surface.

The data in Fig. 15 indicate that in nucleate boiling up to CHF ($20\ \mathrm{K} < \Delta T < 35\ \mathrm{K}$, see Fig. 7) the void fraction decreases sharply when the probe approaches to the heater surface. This can also be observed at $\Delta T = 40$ K in transition boiling. Then the liquid rich layer near the surface gradually disappears if film boiling is approached. The void fraction maximum above the heater is found to be at about 0.5 mm in nucleate boiling, at 0.1 mm at CHF, at 0.05 mm at $\Delta T = 40$ K and it reaches the heater surface at about $\Delta T = 50$ K. The void fractions at the surface in the ΔT region below 50 K are remarkably small. If the data in Fig. 15 are extrapolated to the heater surface, which certainly implies some error, we observe, e.g., at CHF a non-wetted fraction of less than about 15%.

Hohl et al. (1998) presents also data for vapor contact frequencies at the probe tip. The number of vapor contacts increases when the probe is moved towards the heater surface and reaches frequencies as high as 500–600 Hz at about 0.05 mm from the heater surface. It seems that at about these distances the probe detects bubbles from several nucleation sites during their growing period. At larger distances the bubbles coalesce to bigger vapor masses resulting in a decrease of the frequency. A further approach of the probe tip to the surface results in a decrease of the frequency. An explanation could be that at these very small distances the probe tip touches less and less bubbles during their growing period probably at most two because the detected frequencies are less than 100 Hz at nominal tip distances of 0.01 mm to the surface.

In transient boiling the probe measurements were not successful due to the unavoidable thermal expansion and contraction of both the probe and the heater. It turned out that during a transient run the distance between the probe tip and the heater surface varied within a range where the strongest changes in contact frequencies and other quantities occur.

3.4.2. Isopropanol

Buchholz et al. (2004) carried out similar measurements as Hohl et al. (1998), with isopropanol along the boiling curve depicted in Fig. 8. He used the 4-tip probe described in Section 2.5. Results for the void fraction distribution measured with the probe nearest to the surface (probe 1) in different boiling regimes are shown in Fig. 16. Fig. 17 presents a zoom into the plots of Fig. 16 for the heater nearfield region.

The void fraction characteristics are very similar to the findings by Hohl et al. A liquid rich layer very near to the surface is observed. The void fraction at the closest measured distance to the heater (8 μm) increases monotonically from low superheats via CHF to film boiling. Even in transition boiling (40.1 W/cm^2) a decrease of void fraction towards the surface exists. A distinct local maximum of the void fraction distribution occurs in all boiling regimes between moderate nucleate boiling and transition boiling (~40.1 W/cm^2). The

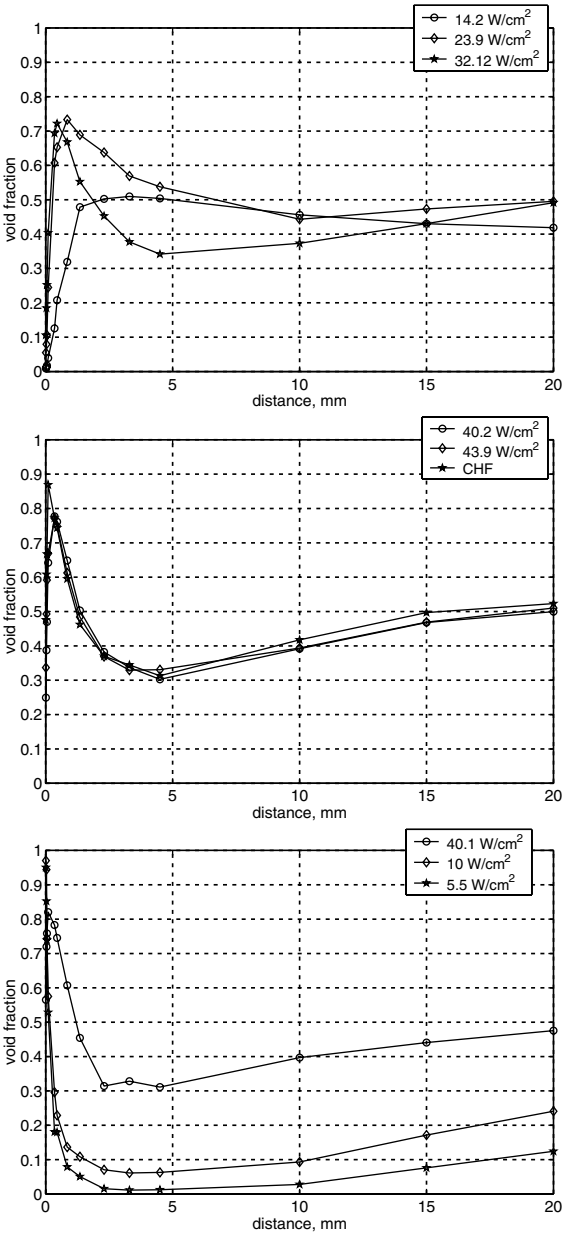

Fig. 16. Mean void fraction of isopropanol for entire distance range to the surface, top: nucleate boiling, middle: nucleate boiling up to CHF, bottom: transition and film boiling. See also boiling curve in Fig. 8.

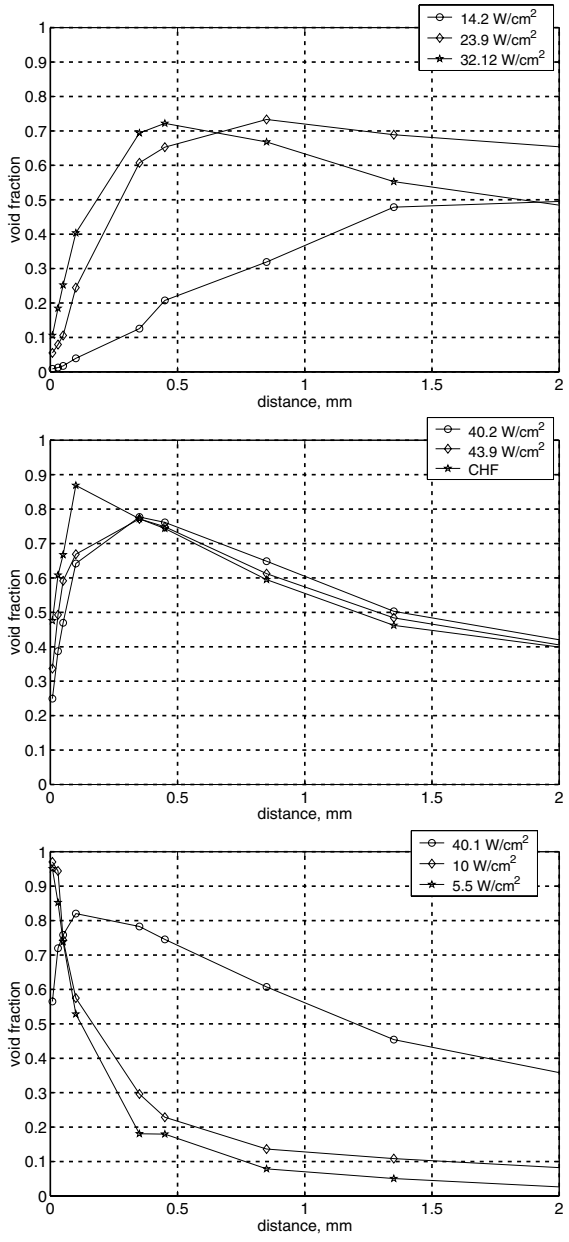

Fig. 17. Mean void fraction of isopropanol for 0–2 mm distance to the surface, top: nucleate boiling, middle: nucleate boiling up to CHF, bottom: transition and film boiling.

distance between the location of the maximum and the heater surface becomes smaller with increasing wall superheat. It is about 0.85 mm at 23.9 W/cm^2 (nucleate boiling) and reaches about 0.1 mm in high heat flux transition boiling (40.1 W/cm^2). Not surprisingly the distances between the maxima and the surface are somewhat larger than in FC-72 boiling since most likely a relation exists between bubble departure diameter d_B and void fraction maximum, and d_B of isopropanol is larger than the one of FC-72.

The void fraction curves exhibit a minimum at a distance of ~4.5 mm between fully developed nucleate boiling and film boiling (Fig. 16). Moreover the void fraction at the largest measured distance (20 mm) is more or less constant (~0.5) between nucleate boiling and CHF. These findings are discussed in the paragraphs on cross correlation later in this chapter. Until now the void fraction data has not been calculated for the other probes of Buchholz' et al.'s 4-tip sensor since huge computation time is required to obtain statistically correct results.

The 4-tip sensor offer the possibility to determine an average interphase velocity in the tip region by cross correlation of the different probe signals. One of the examples presented by Buchholz et al. (2004) is shown in Fig. 18.

Here, the cross correlation coefficients for probe combinations 1/2, 2/3 and 3/4 are plotted for two distances of the lower probe (1) to the surface: 4.5 and 20 mm. Two characteristics are obvious: 1. The larger the distance of the probe ensemble to the surface the better the correlation. In fact, Buchholz et al. report that very weak correlation coefficients are obtained at the smallest distance of 8 μm of the lower probe to the surface. This may be an indication of increasing "disorder" of the two-phase layer towards the surface caused by bubble agitation. 2. The smaller the distance of subsequent probes the better the correlation (note: $1 \rightarrow 2$, 160 μm; $2 \rightarrow 3$, 260 μm; $3 \rightarrow 4$, 330 μm).

The time differences at the peak maxima and the fixed distance between the tips yield an average interphase velocity at the different probe positions above the surface. The velocities are summarized in Table 1 for the region between low superheat nucleate boiling (14.2 W/cm^2 and CHF) for two distances above the heater.

These data is helpful for an interpretation of the void fraction profiles in Figs. 16 and 17. Looking at the

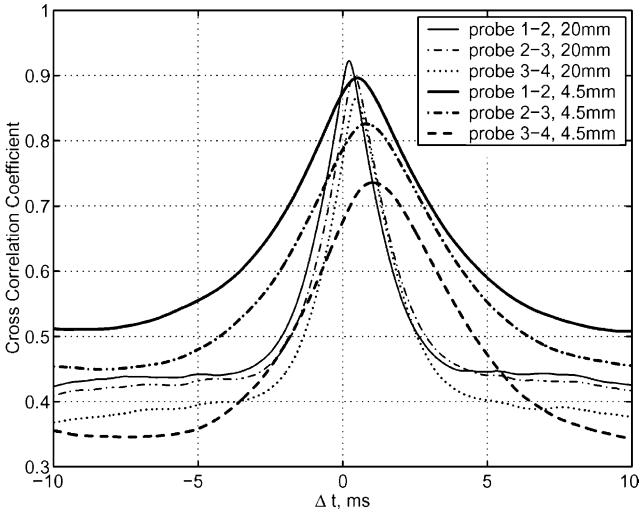

Fig. 18. Cross correlation coefficients for 20 and 4.5 mm distance of the lower probe to the heater surface. Nucleate boiling of isopropanol at 14.2 W/cm^2.

Table 1
Average interface velocity between nucleate boiling and CHF at two probe positions

	Probe 1–2	Probe 2–3	Probe 3–4
Distance between heater surface and lowest probe: 4.5 mm			
$q = 14.2$ W/cm^2	0.31 m/s	0.32 m/s	0.32 m/s
$q = 32.1$ W/cm^2	0.53 m/s	0.58 m/s	0.56 m/s
CHF	0.82 m/s	0.81 m/s	0.81 m/s
Distance between heater surface and lowest probe: 20 mm			
$q = 14.2$ W/cm^2	0.73 m/s	0.66 m/s	0.73 m/s
$q = 32.1$ W/cm^2	0.78 m/s	0.8 m/s	0.82 m/s
CHF	1 m/s	0.98 m/s	1.05 m/s

profiles it is in the first glance surprising that the void fractions at both 4.5 and 20 mm distance are approximately equal between nucleate boiling (32.12 W/cm^2) and CHF though the heat flux and thus the generated mass flow of vapor increases. This is explainable if the velocity rises with increasing heat flux and in fact this trend is proved by the data in Table 1. Furthermore we observe higher velocities at the larger distance (20 mm) and simultaneously an increase of void fraction between 4.5 and 20 mm at a given heat flux (Fig. 16). It seems that the two-phase flow is accelerated in this section above the heater and that in addition a contraction of the bubbly flow area in upward direction occurs. Both effects would increase the measured velocity and also increase the void fraction in upward direction.

Buchholz et al. give no explanation for the strong decrease of void fraction at fixed heat fluxes after the maximum at least in the higher heat flux region. More detailed investigations are required using the huge amount of data available now to give an answer.

4. Mechanistic models

The rather sophisticated experiments with microsensors offer a chance to develop physically based boiling heat transfer models which include phenomena and information explored by the microsensor techniques. A step forward towards physically based models was the microlayer theory (Wayner, 1994; Stephan and Hammer, 1994). One challenge to evaluate this model experimentally is to identify the movement of the contact line at the bottom of a growing bubble. We believe that the highly sensitive microthermocouple array in the center of our heater should be able to identify this movement, at least for larger bubbles in systems with small reduced pressure. Studies of this type will be carried out in the near future.

In boiling regimes at higher heat fluxes up to the critical one and beyond it, the microlayer theory cannot be applied directly to predict heat transfer because of the interaction between bubbles and the dry spot generation beyond CHF, respectively. Nevertheless the idea of evaporation in the contact line region, where the main part of the heat is removed from the heater in a boiling system, can be extended to regions of higher wall superheats as already proposed by Nishio et al. (1998) for the region around CHF. In the following chapter an outline of a model is presented along these lines. It needs data from the microsensor experiments. This holds also for a second model summarized in the subsequent chapter. Here, the instability of a dry spot ensemble on the heater surface is claimed to be the triggering effect for the occurrence of CHF.

4.1. An interfacial-area-density model

Evaporation along the contact line area seems to be the governing mechanism for boiling. This was experimentally proved for the low superheat region (Stephan and Hammer, 1994) and by Nishio et al. (1998), based on visual observations of boiling structures on a thin sapphire heater in the high heat flux region around CHF. Lüttich et al. (2003) propose that this concept should be used for a unifying mechanistic model of the entire boiling curve, because it is reasonable to assume that in other boiling regions the contact line density L_i (length of contact line per unit area) also governs the boiling mechanisms. In transition boiling, for instance, we have the three-phase contact line around the dry spots and in addition many of those lines in the evaporating wet spots. Measurements with optical probes enable to some extent a verification of this modeling concept. Lüttich et al. (2003) use heat transfer data and optical probe data from experiments with FC-72 for this purpose (Hohl et al., 1998; Hohl, 1999, respectively). These results are partly presented in the present report (see boiling curve in Fig. 7 and the void fraction distributions in Fig. 15). A verification with similar data for isopropanol (see Figs. 8, 16 and 17) is not yet finished.

Based on own studies and those from the literature about vapor generation and two-phase kinematics near the heating surface, Lüttich et al. (2003) conclude that the interfacial area density A_i (interfacial area per unit volume) or its flux $A_i v$ (time rate of change of the void

fraction, determined simply by the sum of positive and negative signs of the normal interfacial velocity v) are the governing parameters for evaporation heat transfer. The measurement of A_i would require a four-sensor probe, as theoretically shown by Kataoka and Serizawa (1990). However, Hohl used only a single probe [note that the 4-tip probe used by Buchholz (Section 2.5 of the present report) would not be applicable since the tips are not suitably distributed in space. A suitable probe was not yet designed]. Therefore, the authors were forced to a simplification. According to the studies on the two-phase kinematics mentioned above, there is an indication that the vapor contact frequency f, which was also measured by Hohl with his optical probe, is related to the interfacial contact line density. Hence, Lüttich et al. simply postulate

$$L_i = f(\bar{v}_C)^{-1}, \tag{1}$$

where $\bar{v}_C$ was assumed to be an unknown characteristic average interfacial velocity. It is not useful to apply a more complex concept to allow for the quantities A_i or $A_i v$ since single probe experiments are not able to identify these quantities.

The usefulness of the above concept to correlate heat transfer along the entire boiling curve has been tested by the authors on the basis of a simple geometric model consisting of circular dry spots (vapor stems) on the surface. They are separated in the low superheat region and overlapped at higher superheats. The resulting analytical expressions for contact line density L_i, vapor fraction α_v on the surface, stem diameter d_s and their distance as well as nucleation site density N/A are used to find the functional dependence of this quantities on the superheat ΔT by a parameter identification procedure using the experimental data for α_v and f ($\sim L_i$ according to Eq. (1)) near the surface measured by Hohl. The average velocity $\bar{v}_C$ was assumed to be constant. The identified functions for the quantities mentioned above give reasonable values in all regions along the boiling curve compared with experimental findings. This suggests that the correlation concept for the entire boiling curve based on the contact line density L_i and the contact frequency, respectively, is promising.

Consequently Lüttich et al. postulate a correlation for the boiling heat flux along the entire boiling curve according to

$$q = \frac{C_1}{\bar{v}_C}\Delta T f, \tag{2}$$

where C_1 be a constant allowing for fluid properties, the surface configuration of the heater and other second order parameters. $\bar{v}_C$ was again proposed to be constant. This type of correlation was already assumed by Nishio et al. (1998) for the region around CHF. Eq. (2) includes indirectly the Jacob number Ja, since Ja is defined by ΔT and fluid properties:

$$Ja = \Delta T \frac{\rho_L c_L}{\Delta h_v \rho_v}. \tag{3}$$

In a parameter identification procedure using Hohl's results for $q(\Delta T)$, $f(\Delta T)$ and the vapor fraction $\alpha_v(\Delta T)$ on the surface, Lüttich et al. compared the correlation concept according to Eq. (2) with the classical concept

$$q = q_L(1 - \alpha_v) + q_v\alpha_v \tag{4}$$

proposed by Berenson (1962) for the high superheat region. Comparing the residuals and standard deviations for the parameters in Eqs. (2) and (4) it turns out that the concept according to correlation (2) is superior to the concept used in relation (4) which obviously does not account sufficiently for the governing mechanisms.

The very simple approach by the authors using only one constant ($C_1/\bar{v}_C$ in Eq. (2)) yields a fairly good fit of the measured boiling curve (Fig. 7) as shown in Fig. 19. Note that the subject of this study was simply to prove by means of experimental data that evaporation around contact lines is the governing mechanism along the entire boiling curve. Better predictions of boiling curves require more sophisticated measurements and theoretical studies along the lines of the concept under consideration.

As already outlined, Lüttich et al. came to the conclusion that the interfacial area density A_i or its flux $A_i v$ rather than the contact line density L_i are the governing quantities for the boiling heat flux. Physically this is anyway more consistent since heat cannot be transferred "through a line". In fact there are experimental indications in the literature that at least A_i instead of L_i should be used as correlating parameter. Assuming a simple geometrical model for the two-phase structure at and close to the heated surface consisting of conical vapor stems with a contact angle Φ it holds

$$A_i = L_i(\sin \Phi)^{-1}. \tag{5}$$

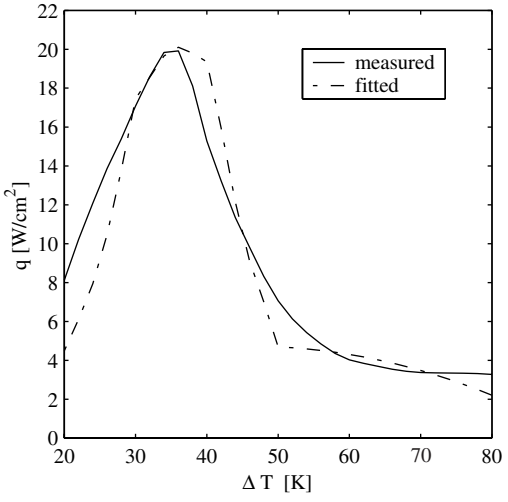

Fig. 19. Measured and predicted (Eq. (2)) boiling curve of FC-72.

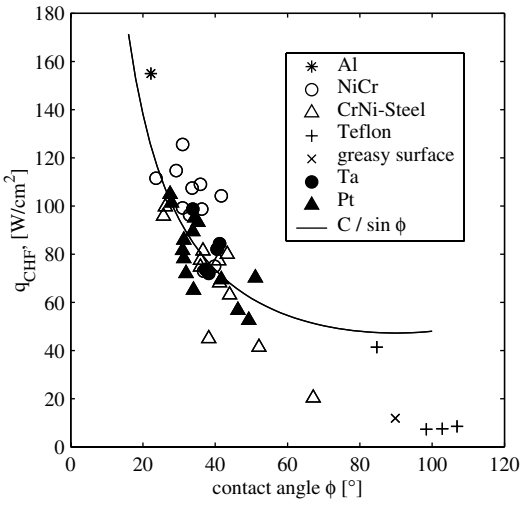

Fig. 20. Influence of contact angle on CHF of boiling water.

Therefore, in boiling experiments where the contact angle is the only parameter changed while all other parameters are kept constant, the heat flux should be proportional to $(\sin \Phi)^{-1}$ if the simplified geometry were correct. There are experimental data by Hahne and Diesselhorst (1978) proving that this trend holds qualitatively at least for CHF.

These authors carried out CHF experiments with water for different contact angles. In Fig. 20 the original data is compared with a least-squares fit according to

$$q_{\mathrm{CHF}} = \frac{C_{\mathrm{CHF}}}{\sin \Phi} \tag{6}$$

with $C_{\mathrm{CHF}} = 47.2$ W/cm^2. Clearly, relation (6) is too simple but it interprets the influence of contact angle Φ correctly. Furthermore this result indicates that at least A_i rather than L_i should be used in models. Hence, Lüttich et al. finally came to the conclusion that modeling efforts along the lines outlined in the present chapter are worthwhile with the objective to refine their first approach to an interfacial-area-density model for the entire boiling curve. However, the game is not over if we would succeed in the development of such a model. We need a more simple access to data like void fraction distribution and contact frequency above the surface because sophisticated experiments with microsensors as described in the present report cannot be carried out for a greater variety of system conditions. Models for such data are required which can be validated by the microsensor data.

4.2. A reaction–diffusion model for the CHF mechanism

The understanding of the phenomenology of critical heat flux (CHF) is still controversial. The most common models, Zuber's (1958) theory of hydrodynamic instability and Haramura and Katto's (1983) macrolayer dryout model are essentially based on hydrodynamic scenarios. Despite a reasonable good agreement between experimental results and predictions of CHF based on these two models, a number of key factors definitely influencing boiling heat transfer and CHF are disregarded in these models (Sadasivan et al., 1995). In particular they do not consider the dynamics of interactions between fluid patterns and heat conduction inside the heater. In order to address this problem, Blum et al. (1999) suggest a novel unifying approach to the development of a mechanistic model for the boiling regimes around CHF based on the mathematical theory of reaction–diffusion systems. They start with the assumption that the macroscopic boiling phenomena, represented by the boiling curve, are caused by the dynamics of formation and propagation of dry spots on the heater surface. The dynamics are caused by the interaction of heat conduction in the heater, the phase transition on the heater surface as well as the fluid dynamics in a small zone close to the heater surface. These highly transient elementary physical phenomena result in the macroscopic non-linear boiling curve if suitable space and time averaging is carried out.

This modeling approach distinguishes two different classes of elementary phenomena, namely the formation of dry spots on the one hand and their stability and dynamics on the other hand. The study is not focused on the former phenomenon but it assumes that dry spots of certain geometrical extension have occurred by some of the mechanisms (e.g. macrolayer dryout, hydrodynamic instability) discussed in the literature. Clearly, a further evaluation of our optical probe results and microthermocouple data can improve our knowledge of this phenomenon. The authors' focus is on the stability of an instantaneously existing ensemble of dry spots on the boiling surface. The model assumptions are depicted in Fig. 21.

The behavior of the flat heater of thickness l is governed by the heat conduction equation in three spatial dimensions (x, y, z). External heating, $q_{\mathrm{H}}(t)$, and heat removal by boiling, $q_{\mathrm{B}}(\vartheta/\Gamma_B)$, occur on opposite sides of the heater element. The peripheral surface Γ_A of the heater is assumed to be adiabatic. The heat flux

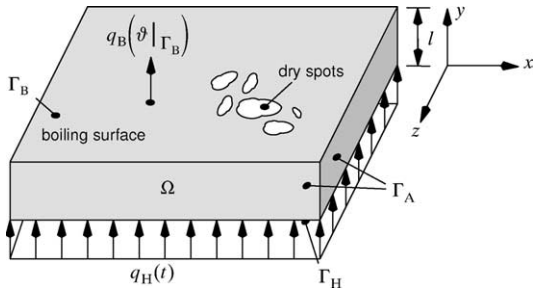

Fig. 21. Heater with dry spots on the surface.

$q_B(\vartheta/\Gamma_B)$ on the heater surface, representing spatio-temporally varying heat transfer, depends (among other factors) on the liquid and vapor contacts at the boiling surface. For simplicity, the authors assume a linear relation between heat flux and temperature difference with different slopes in different boiling regimes, as boundary conditions.

The resulting model consists of the heat conduction equation with material constants and suitable boundary and initial conditions. Unfortunately, analytic results on spatio-temporal patterns which reflect the dynamics of dry spots are not yet available for the three-dimensional case. The attention is therefore restricted to thin heaters with $1 \to 0$ to allow for one- or two-dimensional modeling.

The main results from this study can be summarized as follows: A dry spot expansion is accompanied by a temperature wave in the surface region of the heater. Necessary conditions for the occurrence of such temperature waves have been identified by applying known results from the theory of reaction–diffusion problems as well as by numerical simulation. The investigations show that a single dry spot can only cause the transition to film boiling for thin heaters such as wires or foils. For instance, a dry spot of an extension of only some tenth of a mm is necessary in case of a thin copper heater (0.1 mm thick) at a heat flux of $q_H = 9 \times 10^5$ W/m^2 at water pool boiling to trigger a temperature wave and, hence, CHF (see also Fig. 22).

With increasing thickness of the heater the explanation of a single dry spot causing transition from nucleate to film boiling looses its plausibility. For example, a dry spot of an extension of more than 8 mm would be required in the same system in case of a copper heater of 10 mm thickness to cause this effect.

It is further shown that the size of dry spots required to trigger CHF is diminished tremendously if a number of cooperating dry spots are assumed to exist on the boiling surface. In the upper part of Fig. 22 regular distributed dry spots of size 2δ and distance β and the corresponding temperature profile on the surface are assumed. The result for a heated copper foil of thickness $l = 0.1$ mm is shown in the lower part of Fig. 22. Given a heat flux q_H of, say, 3×10^5 W/m^2 the system is stable up to a maximum dry spot size of $2\delta \approx 3.5$ mm if only one single dry spot exists ($\beta \to \infty$). For several dry spots with a distance of, say, $\beta = 3$ mm the system becomes unstable and CHF is triggered if the dry spot size exceeds $2\delta \approx 0.4$ mm.

The results for thick heaters and for cooperating dry spots mentioned above have been obtained by numerical or analytical computations with simplified heater models. Future work will concentrate on numerical stability analysis of a three-dimensional heater. Powerful adaptive numerical methods, which are not available to date, are a prerequisite to success for this approach. Such results combined with an understanding of the mechanisms of dry spot formation could lead

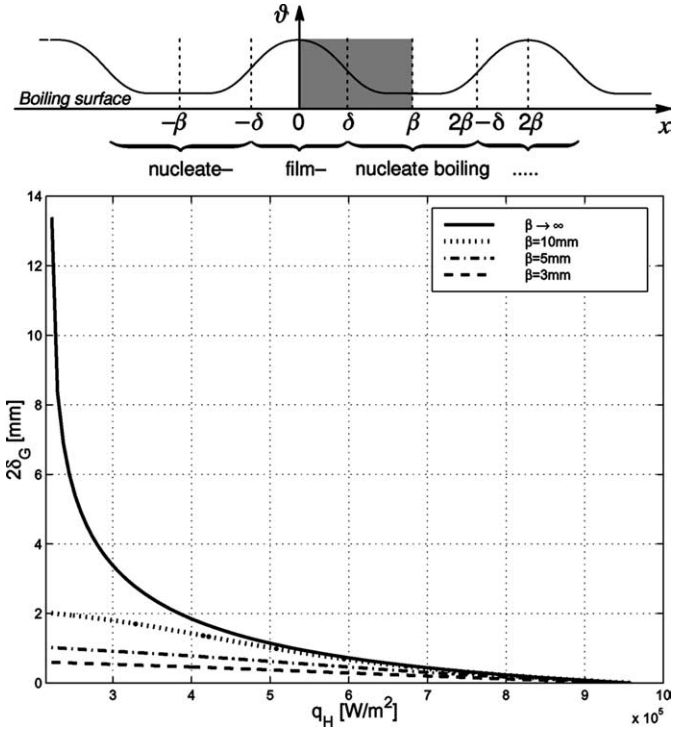

Fig. 22. Distribution of dry spots and stability limits for water pool boiling on a copper foil with 0.1 mm thickness.

to a physically sound mechanistic model for CHF under steady-state and transient heating conditions. A substantial help on the way towards this model will be data from multitip-optical probes and microthermocouples. However, the same holds as mentioned in Section 4.1: We need a simplified access to data like dry spot sizes and dynamics. Models for such data are required which can be validated by the microsensor data.

5. Conclusions

Based on all the presented results the following conclusions can be drawn on the behavior of boiling curves, on some mechanisms of heat transfer in the different boiling regimes and on some new aspects of modeling the heat transfer in boiling.

5.1. Boiling curves under steady-state and transient conditions

Under steady-state pool boiling conditions with a good control system to stabilize boiling in the transition region and a clean heater surface, no hysteresis has been observed in the transition region for both well wetting fluids and fluids with a larger contact angle. Small disturbances in the transition boiling curve have been observed with water and isopropanol. This may result from a non-ergodic boiling behavior on the heater surface. Clusters of dry patches occur which change their configuration with the wall superheat. The size of the clusters is smaller than the heater surface area. It is unlikely that the clustering effect is caused by insufficient controlling but we are not yet able to give a physical/mathematical explanation of this effect. For a surface with contamination, boiling curves are not reproducible.

Under transient conditions a hysteresis is observed: Heating transients yield always higher heat fluxes than cooling transients at the same wall temperature. At fast transients enormous differences in the heat fluxes compared with the steady-state case have been observed.

A comparison of optical probe signals and microthermocouple signals (Hohl and Auracher, 2000; Hohl, 1999) in steady-state FC-72 experiments enables an estimate of the density of nucleation sites. It turns out, e.g., that the minimum nucleation site density near CHF is about 3×10^8 m^{-2}. Regarding the uncertainty of this estimate we may conclude that the nucleation site density is between 10^8 and 10^9 m^{-2}. This is in the order of magnitude of the results by Pinto et al. (1996), who observed 4×10^7 nucleation sites per m^2 in propane boiling at a heat flux of 5 W/cm^2, which is below CHF.

The high density of active nucleation sites in the region between fully developed nucleate boiling and CHF and the resulting highly turbulent two-phase boundary layer let us conclude that the strong increase of heat flux in heating transients and vice versa in a cooling process is mainly due to the intensive two-phase convection heat transfer from the wall to the bulk. Note that this is most likely not primarily because of a change in the two-phase structure (i.e., nucleation site density, bubble frequency, void fraction distribution etc.) near the wall, which is not significantly affected by temperature transients (see Section 3.3). Rather, it is mainly due to the instantaneous temperature gradient in the fluid at the heater surface which is increased or decreased during the transient modes. Hence, the highly turbulent microconvective transfer of energy is intensified if it takes place in a temperature field with steeper gradients caused by transient heating or with weaker gradients in the cooling mode. Clearly, we have no direct experimental indication for steeper or weaker temperature gradients during the transients. Furthermore our measurements of the two-phase structure near the wall and its behavior during transients are not precise enough to exclude an error in the above statement. Therefore, more precise measurements along the line presented in this report should be carried out to support this conclusion. Besides, an estimate reveals that unsteady-state heat conduction to the liquid cannot explain the strong increase of heat flux during a heating transient.

The results obtained with microthermocouples (Hohl and Auracher, 2000; Hohl, 1999) let us furthermore assume that at wall superheats beyond CHF the two-phase structure at a given wall superheat is not independent of the heating or cooling rate. The faster the transient the stronger the delay in the two-phase structure formation. This could be one reason for the deviation of heat flux between the transient and steady-state case in the transition and film boiling region. But we need more experiments with our microsensors to gain a better insight in the physics responsible for this deviation.

5.2. The structure of the macrolayer

The data by Hohl et al. (1998) with F-72 and the more recent measurements by Buchholz et al. (2004) with isopropanol (both see Section 3.4) give us now a much clearer insight in the nearfield region above the boiling surface (see Figs. 15–17). As several authors assume, there is a liquid rich layer. The void fraction is very small at the surface but with increasing tendency towards higher superheats. It is quite reasonable that this "surface vapor fraction" is associated with the non-evaporating area in the center of attached bubbles. With increasing superheat the surface fraction of these

areas increases because of the increase of active nucleation sites. Already before reaching CHF some bigger dry patches occur probably due to coalescence effects on the surface, as observed by Buchholz et al. (2004). Away from the surface the void fraction increases until a maximum is reached. This may be explained as follows: Assuming the region between surface and void fraction maximum is the one of growing but attached bubbles. Then we would measure in the time and space average (i.e. in the ergodic case) an increase in void fraction in direction away from the surface. Assuming a departure diameter d_B and imagine a layer at a distance of $d_B/2$, cutting bubbles still growing, and those which are departing, then we would measure the maximum void fraction not necessarily at a distance $d_B/2$ but likely not far away from it. Anyway, the peak distance to the surface is most likely related to the departure diameter. This is supported by the observation that peak distances to the surface of F-72 (Fig. 15) are smaller than those of isopropanol (Fig. 17) and this holds also for the departure diameters of both fluids. It was furthermore observed that the peak distances to the surface for both fluids decrease with increasing wall superheat. Having the above model in mind this might be an indication that with increasing superheat the bubble shape becomes more and more flat, i.e. extended parallel to the surface during the growing period. Studies in the literature support this conclusion (e.g. Mitrovic, 1985). An explanation of the decrease in void fraction after the peak which was observed in the FC-72 experiments (Fig. 15) and especially in the more extended measurements with isopropanol (Figs. 16 and 17) is in a first glance not easy to explain. More detailed analyses are required to find an answer.

The existence of stationary vapor stems in the liquid rich area (macrolayer) is rather unlikely, as always, even at the smallest distances, very short vapor contacts have been detected. Even the very thin tip (<1.5 μm) of Buchholz' et al.'s, probe did not observe signal characteristics which would indicate a vapor stem structure near the surface. The macrolayer region is obviously quite agitated in the higher heat flux regions. Hohl and Auracher (2000) observed in the FC-72 experiments at a distance of 0.05 mm from the heater up to 600 vapor contacts per second. Active nucleation sites are not locally fixed for a longer period. The activation and deactivation seems to occur within a wide frequency range.

5.3. Mechanistic models

The experimental results with microsensors confirm that evaporation in the contact line region, where the main part of heat is removed from the heater surface, is a promising modeling concept for the entire boiling curve. Studies by Lüttich et al. (2003) propose that the interfacial area density A_i rather than the contact line density L_i should be used as governing modeling parameter since A_i accounts also for the contact angle between fluid and surface. It seems that the contact frequency measured near the surface by an optical probe is a good measure for the contact line density. But better results, namely those for A_i, can be expected if measurements with a 4-tip probe with the tips properly distributed in space are available.

The microsensor experiments can also contribute to a more physically sound model for CHF. Blum et al. (1999) propose a model based on the mathematical theory of reaction–diffusion systems. Their concept is that heat transfer in the CHF region is caused by the dynamics of formation and propagation of dry spots on the heater surface. The dynamics are caused by the interaction of heat conduction in the heater, the phase transition on the heater surface as well as the fluid dynamics in a small zone close to the heater surface. The authors concentrate not on the formation of dry spots but on their stability and dynamics. Finally it can be shown under simplified mathematical conditions that for a given ensemble of dry spots on the heater surface a stability limit exists at which the dry spots start to grow and trigger CHF. This model requires experimental information on the size and dynamics of dry spots on the surface, like the data extracted by Buchholz et al. (2004), from their microthermocouple experiments. Clearly, we need also an answer—in terms of a good model—about the formation of dry spots on the surface. Until now, this problem is not included in Blum's et al.'s theory.

5.4. Needs for further studies

Measurements with microsensors in the nearfield above and below the heater surface yield key data for the development of mechanistic models for boiling in the different regimes. The results presented in the present report contribute already to some steps forward in the understanding of this very complex process. There are still a lot of already collected raw data waiting to be evaluated to give more precise answers to

- dry spot geometry, dynamics and stability;
- the space- and temporal-distribution of temperature and heat flux at the surface;
- the two-phase behavior above the heater to explain the void fraction distribution in the steady-state case and the boiling curve characteristics under transient conditions;
- other problems mentioned in the text.

However, the game is far from being over if we find the above mentioned answers. We need

- experiments with other fluids to solicitate the existing findings;
- a special 4-tip probe to evaluate the interfacial area density near the surface and models to predict this quantity;
- realistic models for the macrolayer above the heater;
- models for the formation of dry spots in the higher superheat regions, etc.

We are convinced that substantial progress is only possible if we tackle the problem from both the experimental and the theoretical end. Preferably, both approaches should be closely linked.

We studied here only boiling-phenomena on smooth surfaces. Heat transfer enhancement by structuring the surfaces has already a long history. Most of the basic phenomena occurring at smooth surfaces are also relevant at enhanced surfaces, but several additional problems have to be solved in these cases. Last but not least, in practical applications we have quite often boiling mixtures which bring some more parameters into the game. In summary there is still a lot to do but real progress requires studies of the fundamentals.

Acknowledgements

The authors highly appreciate financial support by the ''Deutsche Forschungsgemeinschaft, DFG'' in the frame of a joint research project on fundamentals of boiling heat transfer. They are also very grateful for the tremendous work of their doctoral students J. Blum, M. Buchholz, R. Hohl, and T. Lüttich.

References

Auracher, H., Marquardt, W., 2002. Experimental studies of boiling mechanisms in all boiling regimes under steady-state and transient conditions. Int. J. Therm. Sci. 41, 586–598.

Berenson, P.J., 1962. Experiments on pool-boiling heat transfer. Int. J. Heat Mass Transfer 5, 985–999.

Blum, J., Marquardt, W., 1997a. An optimal solution to inverse heat conduction problems based on frequency domain interpretation and observers. Numer. Heat Transfer, Part B. Fundamentals 32, 453–478.

Blum, J., Marquardt, W., 1997b. Robust and efficient solution of the inverse heat conduction problem using observers. Advanced Concepts and Techniques in Thermal Modelling. In: Proc. of Eurotherm Seminar, vol. 53, pp. 175–182.

Blum, J., Marquardt, W., Auracher, H., 1996. Stability of boiling systems. Int. J. Heat Mass Transfer 39, 3021–3033.

Blum, J., Lüttich, T., Marquardt, W., 1999. Temperature wave propagation as a route from nucleate to film boiling. In: Celata, G.P., DiMarco, P., Shah, R.K. (Eds.), Two-Phase Flow Modelling and Experimentation. Edizioni ETS, Pisa, pp. 137–144.

Buchholz, M., Auracher, H., Lüttich, T., Marquardt, W., 2004. Experimental investigation of local processes in pool boiling along the entire boiling curve. Int. J. Heat Fluid Flow, this issue. doi:10.1016/j.ijheatfluidflow.2003.11.020.

Buchholz, M., Auracher, H., Lüttich, T., Mhamdi, A., Marquardt, W., 2001. Pool boiling heat fluxes (part I): local temperature and heat flux fluctuations at the heater surface. In: Proc. IIR-Conf., Com. B1, Thermophysical Properties and Transfer Processes, October 3–5, Paderborn, Germany.

Buchholz, M., Lüttich, T., Auracher, H., Marquardt, W., 2000. Steady-state pool boiling experiments with water between nucleate and film boiling. In: Proc. 3rd Europ. Thermal Sciences Conf., Heidelberg, Germany, paper 3–10.

Hahne, E., Diesselhorst, T., 1978. Hydrodynamic and surface effects on the peak heat flux in pool boiling. In: Proc. 6th Int. Heat Transfer Conference, Toronto, vol. 1.

Haramura, Y., Katto, Y., 1983. A new hydrodynamic model of critical heat flux, applicable widely to both pool and forced convection boiling on submerged bodies in saturated liquids. Int. J. Heat Mass Transfer 26, 389–399.

Hohl, R., 1999. Mechanism des Wärmeübergangs bei stationärem und transientem Behältersieden. In: VDI Fortschritt-Berichte, vol. 3/597, VDI, Düsseldorf, Germany.

Hohl, R., Auracher, H., 2000. Transient pool boiling experiments. In: Mayinger, F., Giernoth, B. (Eds.), Transient Phenomena in Multiphase and Multicomponent Systems. Wiley-VCH-DFG, New York, pp. 241–256.

Hohl, R., Auracher, H., Blum, J., Marquardt, W., 1998. Characteristics of liquid–vapor fluctuations in pool boiling at small distances form the heater. In: Heat transfer 1998. In: Proc. 11th Int. Heat Transfer Conf., vol. 1, pp. 383–388.

Hohl, R., Blum, J., Buchholz, M., Lüttich, T., Auracher, H., Marquardt, W., 2001. Model-based experimental analysis of pool boiling heat transfer with controlled wall temperature transients. Int. J. Heat Mass Transfer 44, 2225–2238.

Kataoka, I., Serizawa, A., 1990. Interfacial area concentration in bubbly flow. Nucl. Eng. Design 120, 163–180.

Lüttich, T., Marquart, W., Buchholz, M., Auracher, H., 2003. Towards a unifying heat transfer correlation for the entire boiling curve. In: Proc. 5th Int. Conf. on Boiling Heat Transfer, 4–8 May, Montego Bay, Jamaica.

Luke, A., Gorenflo, D., 2001. Microstructure of evaporator surfaces and database for roughness, bubble formation and heat transfer. In: Proc. IIR-Conf., Com. B1, Thermophysical Properties and Transfer Processes, October 3–5, Paderborn, Germany.

Mitrovic, J., 1985. Wärmetransport in der Umgebung einer wachsenden Dampfblase. Wärme und Stoffübertragung 19, 47–52.

Nishio, S., Gotoh, T., Nagai, N., 1998. Observation of boiling structures in high heat-flux boiling. Int. J. Heat Mass Transfer 41, 3191–3201.

Pinto, A., Gorenflo, D., Künstler, W., 1996. Heat transfer and bubble formation with pool boiling of propane at a horizontal copper tube. in: Proc. 2nd Europ. Therm. Sci. Conf. ETS, Pisa, vol. 3, pp. 1653–1660.

Sadasivan, P., Unal, C., Nelson, R., 1995. Perspective: issues in CHF modelling—the need for new experiments. ASME J. Heat Transfer 117, 558–567.

Silverman, L., 1969. Inversion of multivariable linear systems. IEEE Trans. Automatic Control 14 (3), 270–276.

Stephan, P., Hammer, J., 1994. A new model for nucleate boiling heat transfer. Wärme und Stoffübertragung 30, 119–125.

Ungar, E.K., Eichhorn, R., 1996. Transition boiling curves in saturated pool boiling from horizontal cylinders. J. Heat Transfer 118, 654–661.

Varga, A., 1999. Model reduction routines for SLICOT. Technical Report NICONET Report 1999-8, Working Group on Software WGS, ESAT-Katholieke Universiteit Leuven.

Wayner Jr., P.C., 1994. Thermal and mechanical effects in the spreading of a liquid film due to a change in the apparent finite contact angle. J. Heat Transfer 116, 938–945.

Witte, L.C., Lienhard, J.H., 1982. On the existence of two transition boiling curves. Int. J. Heat Mass Transfer 25, 771–779.

Zuber, N., 1958. On the stability of boiling heat transfer. ASME J. Heat Transfer 80, 711–720.